Letter | Editors' Suggestion

Anisotropic cage evolution in quasi-two-dimensional colloidal fluids

Noman Hanif Barbhuiya and Chandan K. Mishra*
Department of Physics, Indian Institute of Technology Gandhinagar, Palaj, Gandhinagar, 382055, Gujarat, India

(Received 10 August 2024; accepted 5 November 2024; published 12 December 2024)

We experimentally explore the morphological evolution of cages in quasi-two-dimensional suspensions of colloidal fluids, uncovering a complex dynamic restructuring in the fluid. Although cages display isotropic evolution in the laboratory frame, we observe a striking anisotropy when analyzed in the displacement frame of the caged particles. Moreover, our findings reveal that particles in specific but distinct regions of the cage predominantly contribute to either its persistence or relaxation. Thus, our study provides a coarse-grained microscopic picture of the structural relaxation of these fluids through cage evolution, which has broader implications for the flow and phase behavior of complex fluids in confined geometry.

DOI: 10.1103/PhysRevE.110.L062602

Cage formation, whether transient or long-lived, is a fundamental feature of condensed matter systems such as (supercooled) liquids & glasses [1–5] and crystals [6,7]. Microscopic insights into the structural configuration and dynamical evolution of cages have offered crucial understandings of diverse phenomena, such as the rheological [8] and mechanical properties [4] of the materials, as well as about dynamical phases of a system [9,10]. For example, the distinct nature of glass transition and prediction of crystal melting in two dimensions (2D) compared to three dimensions (3D), becomes dimension-agnostic when the dynamics of particles relative to their respective cages, rather than their self-dynamics, are considered [11–15]. This is because long-wavelength Mermin-Wagner fluctuations, which influence the dynamics in 2D systems, are believed to be accounted for in the cage-relative perspective [11–14].

Interestingly, recent studies suggest that long-wavelength Mermin-Wagner fluctuations are also present in 2D colloidal liquids and lead to the violation of the ubiquitous Stokes-Einstein relation, which connects the microscopic diffusivity of the tracers and the bulk viscosity of the liquid [16]. Once again, the cage-relative dynamics of the particles have been shown to restore the usual behavior of the Stokes-Einstein relation for 2D liquids [16]. However, despite the extensive exploration of cage-relative dynamics, the evolution of the cages themselves in 2D colloidal fluids—their transient nature leading to possible changes in their shape over time, which consequently dictates the structural relaxation of the fluid—has never been explored. It is particularly intriguing as long-wavelength fluctuations have been alluded to stem from hydrodynamic interactions [16,17], which are direction-dependent in the body frame of particle-pair for quasi-two-dimensional (q2D) colloidal fluids [18]. Thus, the coarse-grained depiction of fluid dynamics at the lengthscale of the cages can elucidate the structural relaxation of fluids in confined geometries by examining the dynamic restructuring of cages under emergent hydrodynamic interactions.

In this letter, we employ video microscopy to experimentally investigate the spatiotemporal evolution of particles forming the cages in quasi-two-dimensional (q2D) colloidal fluids, both in the laboratory and in the displacement frame of the reference caged-colloid. As expected, the fraction of particles that remain part of the reference caged-particle, defined at the initial time t_0 decreases exponentially over time, facilitating the structural relaxation of the fluid. Notably, the observed size of cages over the cage-relaxation timescales suggests that their morphological evolution is strongly influenced by near-field hydrodynamic interactions in q2D confinement (Fig. 1) [18]. As a result, while the mean shape of the cages appears to evolve isotropically in the laboratory frame of reference, their evolution is anisotropic and asymmetric in the displacement frame of the reference caged-particle (Fig. 2). Finally, consistent with hydrodynamic motional modes, we identify distinct hotspots within the initial cage structure, where particles either contribute to cage persistence or facilitate cage relaxation, thereby unraveling the crucial role of cages in the structural relaxation of the fluid (Fig. 3).

Aqueous suspension of charge-stabilized polystyrene colloidal particles, diameter: $\sigma = 1.04$ μm, polydispersity ∼3%, were loaded in a wedge-shaped cell, which was then allowed to stand vertically for particles to sediment under gravity and form a monolayer in the quasi-two-dimensional region of the cell [18]. Once a desired area fraction was achieved, the cell was equilibrated for several hours under the microscope. After equilibration, video microscopy was performed for 20 minutes using 100x oil objective (1.4 numerical aperture) at 10 frames per second (fps) using the Hamamatsu ORCA-Flash 4.0 camera. We have captured data in the liquid regime at five area fractions ϕ in the range $0.15 \leqslant \phi \leqslant 0.35$, in the same region of the cell [19]. The trajectory of each particle was determined using standard image processing and tracking algorithms [20]. The dynamic spatial resolution in our experiments was 20 nm.

*Contact author: chandan.mishra@iitgn.ac.in

 ©2024 American Physical Society

The identity of cage particles $C(i,t)$ for i^{th} particle at a time t is determined using Voronoi tessellation, which partitions the 2D space into neighborhoods (cells) around each particle such that every point within a cell is closer to the particle than to any other particle [Fig. 1(a)] [21]. In other words, the cage particles constitute the nearest-neighbor envelope as determined by Voronoi tessellation. The order of $C(i,t)$, $n(C(i,t))$, represents the number of particles forming the cage of the i^{th} particle that is also equal to the number of vertices in its Voronoi cell. With time, the identity of particles contained in $C(i,t)$ changes, leading to the relaxation of the cage and, consequently, the structural relaxation of the fluid.

The relaxation (or persistence) time of the cage is measured by calculating the ensemble-averaged fraction of common cage particles $\langle f(\Delta t)\rangle$ with lag time Δt, $\langle f(\Delta t)\rangle = \frac{1}{N}\left\langle \sum_i^N \frac{n(C(i,t_0)\cap C(i,t_0+\Delta t))}{n(C(i,t_0))}\right\rangle_{t_0}$. Here, $\langle\cdot\rangle_{t_0}$ represents initial time averaging over t_0, corresponding to a given Δt, and N is the total number of particles. $\langle f(\Delta t)\rangle$ exhibits a stretched-exponential decay and yields the persistence (or relaxation) time of the cage, τ_{cage} [Fig. 1(b)]. For the range of ϕ studied, $\tau_{\text{cage}} \sim 10$ s and, surprisingly, does not seem to change with ϕ. This suggests that for the range of ϕ studied in this work, the coarse-grained structural relaxation of the fluid over the lengthscales of the cages, typically associated with their bulk relaxation, may be density-independent.

Next, to probe the spatial extent or lengthscales associated with cage relaxation, we have measured the radius of gyration R_g of the cages at $\Delta t = \tau_{\text{cage}}$. $R_g(i,\Delta t)$, measured from the positions of particles at $t_0+\Delta t$, which forms the cage of i^{th} particle at t_0, is defined as $R_g(i,\Delta t) = \sqrt{\frac{1}{n(C(i,t_0))}\sum_{c_j\in C(i,t_0)}(\mathbf{r}_j(t_0+\Delta t) - \langle \mathbf{r}_j(t_0+\Delta t)\rangle_j)^2}$. Here, $\mathbf{r}_j(t_0+\Delta t)$ is the position of the j^{th} particle belonging to the set of particles that form the cage of i^{th} particle at t_0. Note, throughout the letter, the sets and their elements are represented using uppercase and lowercase alphabets, respectively. The distribution of R_g, $P(R_g)$, shows a Gaussian profile and yields the average radius of gyration of cages $\langle R_g\rangle$ [inset to Fig. 1(c)]. As expected, $\langle R_g\rangle$ decreases with increasing ϕ [Fig. 1(c)]. More importantly, the average cage size over the τ_{cage} turns out to be $\sim 2-3\sigma$ [Fig. 1(c)], implying that the temporal evolution of cages should be strongly governed by the nature of near-field hydrodynamic interactions in q2D spatial confinement, which is direction-dependent (anisotropic) in the body frame of colloid-pairs [18].

To directly demonstrate that hydrodynamics is crucial in the evolution of the cages, we investigate how the motion of the reference caged-particle influences the motion of its surrounding neighbors. In other words, we measure the two-particle hydrodynamic displacement correlations $H^{L,T}_{\text{cage}}(\Delta t)$ between the reference caged-particle and its surrounding nearest-neighbors forming the cage, along longitudinal (L) and transverse (T) directions, defined by $H^{L,T}_{\text{cage}}(\Delta t) = \left\langle \frac{1}{N}\sum_i^N \left(\frac{1}{n(C(i,t_0))}\sum_{c_j\in C(i,t_0)} \Delta\mathbf{r}_i^{L,T}(\Delta t)\cdot\Delta\mathbf{r}_j^{L,T}(\Delta t)\right)\right\rangle_{t_0}$. The L and T directions are defined in the body frame of the pair of particles, always composed of the reference caged-particle and any particle forming its cage, such that L is along the line joining the pair at t_0, while T is perpendicular to it. $\Delta\mathbf{r}_i^{L,T}(\Delta t)$ is the displacement of the i^{th} particle along the L or T over Δt, and $\langle\cdot\rangle$ denote an average over all t_0. Reminiscent with the direction-dependent (anisotropic) nature of hydrodynamic interactions in quasi-2D colloidal fluids [18], we find that for all the $\Delta t \leqslant \tau_{\text{cage}}$, $H^L_{\text{cage}}(\Delta t) > 0$ and $H^T_{\text{cage}}(\Delta t) < 0$ (Table S1 of the Supplemental Material (SM)) [22]). Thus, the temporal evolution of the cages is strongly influenced by near-field hydrodynamics, which may lead to a distinctive evolution of cages and consequently dictate the dynamic restructuring of the fluid.

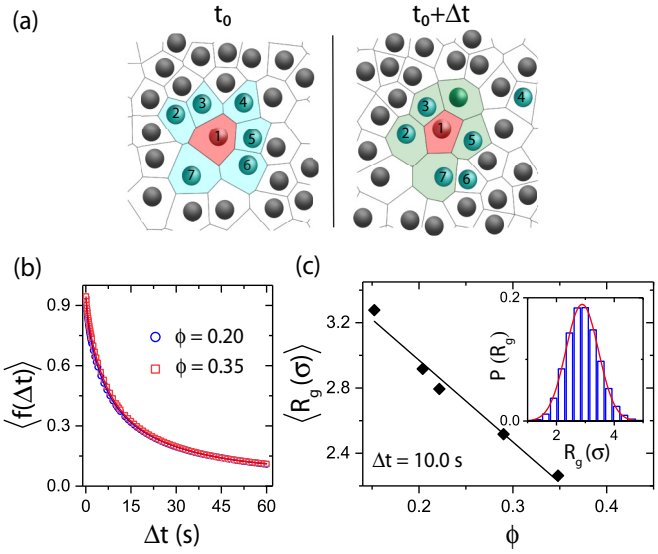

FIG. 1. Cage characterization in quasi-two-dimensional colloidal fluids. (a) Rendering of the Voronoi cells (polygons) for a representative subset of particles (spheres) in the experimental field of view at initial, t_0 (left), and later time, $t_0+\Delta t$ (right) at $\phi = 0.35$, with $\Delta t = 2.5$ s. The representative reference caged-particle's (red sphere) Voronoi cell with its adjoining cells at t_0 (cyan polygons) and $t_0+\Delta t$ (green polygons), determines the identity of the particles forming the cage (shown as numerals on the spheres). (b) Average fraction of common cage particles $\langle f(\Delta t)\rangle$ versus lag time Δt for area fractions, $\phi = 0.20$ (blue circles) and $\phi = 0.35$ (red squares). (c) The average radius of gyration of the cages $\langle R_g\rangle$ in the units of σ versus ϕ for $\Delta t = \tau_{\text{cage}}$ with the solid line as a guide to the eye. The standard error of mean of $\langle R_g\rangle$ is less than the symbol size. Inset shows the probability distribution of R_g, $P(R_g)$, for $\phi = 0.20$, and $\Delta t = \tau_{\text{cage}}$, with the red curve being a Gaussian fit to the data.

As the fluid relaxes, particles of the cage, as defined at t_0, will diffuse and may lead to a change in the shape of the cage. Thus, to capture the microscopic evolution in the shape of the cages with Δt, we plot the probability distribution of the positions of the particles of the cage, $P(\mathbf{r}_j(t_0+\Delta t)|c_j \in C(i,t_0))$, defined at t_0, over Δt [Figs. 2(a)–2(e)]. Here, the argument on the right of the "|" represents the condition applied for the quantity being measured on the left. Note that the probabilities are calculated from the ensembles of particles (and their cages) and, for a given Δt, averaged over t_0. Particles forming the cage spread radially, both outward and inward, from their initial position, with $P(\mathbf{r}_j(t_0+\Delta t)|c_j \in C(i,t_0))$ being symmetric about the center of mass of the cages at t_0.

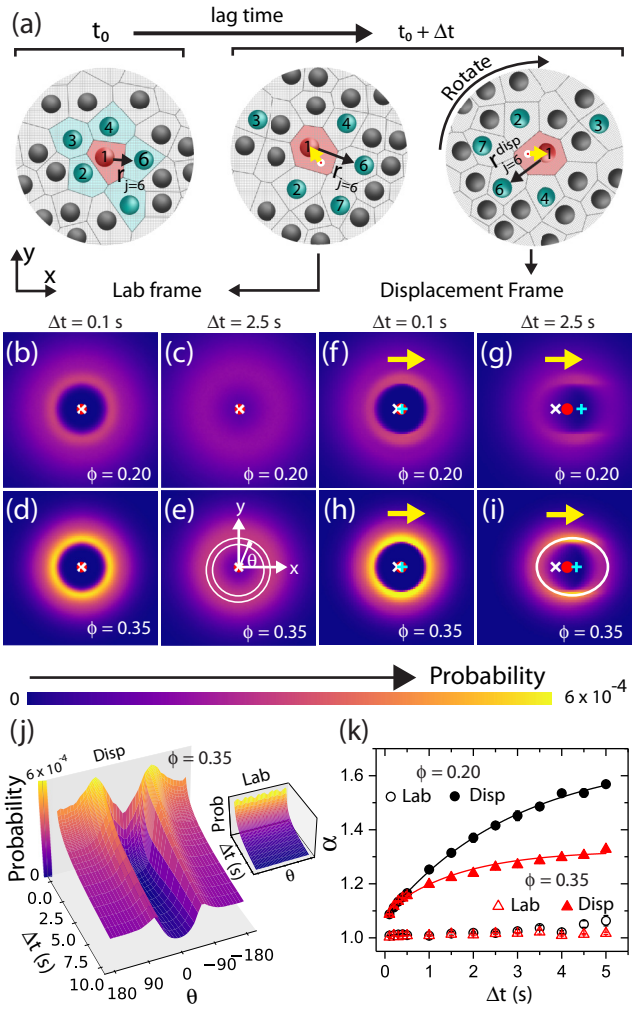

FIG. 2. Cage evolution in quasi-two-dimensional colloidal fluids. (a) Rendering from experiments illustrating the laboratory and displacement frames of reference. Vector joining the reference caged-particle with a representative particle that forms the cage $\mathbf{r}_j$ at every instant is shown in black arrow. The displacement vector of the caged-particle $\Delta\mathbf{r}_i(\Delta t)$ is shown in yellow arrow. The right panel demonstrates the transformation of particle coordinates to the displacement frame, where the displacement of the reference-caged particle (red) is aligned with the x –axis. Ensemble-averaged colormap, (b)–(e) $P(\mathbf{r}_j(t_0+\Delta t)|c_j \in C(i,t_0))$ in the laboratory frame, and (f)–(i) $P(\mathbf{r}_j^{\rm disp}(t_0+\Delta t)|c_j \in C(i,t_0))$ in the displacement frame, for two distinct ϕ and Δt. White cross and red solid circle in (b)–(i) represent the mean of the probability distribution at t_0 and $t_0+\Delta t$, respectively. Cyan plus symbol in (f)–(i) represents the mean position of the reference caged-particle in the displacement frame. Yellow arrows in (f)–(i) show the displacement direction of the reference caged-particle. (j) Total probability within an annular region with $1.00\sigma \leqslant r \leqslant 1.25\sigma$ and centered on the mean of the probability distribution, as a function of angle θ [as illustrated in (e)] and Δt for $\phi = 0.35$, in the displacement frame and laboratory frame (inset). (k) Aspect ratio α of the fitted ellipse along the maxima of the probability distribution as a function of Δt for two distinct ϕ in the laboratory (open symbols) and displacement frames (solid symbols). Data points and their respective error in (k) represent the mean and standard error of α, calculated from four statistically independent time segments of 250 s, out of $\sim 10^3$ s of total experimental time duration.

The diffused annular ring signifies the caging of the particle by its neighbors in colloidal fluids [Figs. 2(b)–2(e)] and, as expected, the annular ring spreads with Δt. For a given Δt, with an increase in ϕ, as caging effects strengthen, the annular ring becomes more localized, as seen in Figs. 2(b)–2(e) and Video 1 of the SM [22].

$P(\mathbf{r}_j(t_0+\Delta t)|c_j \in C(i,t_0))$ is found to be symmetric. However, note that the laboratory frame of measurements of the positions of particles forming the cage for the analysis of $P(\mathbf{r}_j(t_0+\Delta t)|c_j \in C(i,t_0))$ will be unable to capture any possible influence of the unique nature of hydrodynamic interactions in q2D colloidal fluids on the dynamic restructuring of the cages. Hence, to discern the effects of hydrodynamics on the evolution of the shape of the cages, we calculate $P(\mathbf{r}_j^{\rm disp}(t_0+\Delta t)|c_j \in C(i,t_0))$ in the displacement frame of the i^{th} reference caged-particle. Here, we rotate the positions of all the particles of the cages such that the displacement of reference-caged particle aligns along the x –axis [Fig. 2(a)]. In essence, we transform $\mathbf{r}_i$ in the laboratory frame to $\mathbf{r}_i^{\rm disp}$ in displacement frame by $\mathbf{r}_i^{\rm disp} = \mathbf{R}(-\psi)\mathbf{r}_i$, where ψ is the angle that the displacement of the reference caged-particle subtends with x –axis and $\mathbf{R}(-\psi)$ is the rotation matrix with elements $R_{lm}(\psi) = \cos(\psi)\delta_{lm} + \sin(\psi)\delta_{lm}$.

Interestingly, unlike $P(\mathbf{r}_j(t_0+\Delta t)|c_j \in C(i,t_0))$, $P(\mathbf{r}_j^{\rm disp}(t_0+\Delta t)|c_j \in C(i,t_0))$ deviates from the symmetric annular shape and is no longer isotropic with probability densities being different in distinct regions [Figs. 2(f)–2(i) and Video 1 of the SM [22]]. To quantify this localization of the probabilities, we calculate the net probability within an annular region with an inner and outer radius of 1.00σ and 1.25σ, and centered on the mean of the probability distribution, as a function of angle θ [for example, see Fig. 2(e)]. For a fixed ϕ, while the net probability is constant for all θ for $P(\mathbf{r}_j(t_0+\Delta t)|c_j \in C(i,t_0))$ [inset to Fig. 2(j)], however, it displays two maxima at $\theta \sim \pm 90$ for $P(\mathbf{r}_j^{\rm disp}(t_0+\Delta t)|c_j \in C(i,t_0))$ [Fig. 2(j)]. It indicates an accumulation of particles forming the cage in regions perpendicular to the motion of the caged-particle, which is in concordance with the dipolar nature of hydrodynamics in q2D colloidal fluid.

To further quantify the anisotropy in $P(\mathbf{r}_j^{\rm disp}(t_0+\Delta t)|c_j \in C(i,t_0))$, we fit an ellipse along the maxima of the probability distribution [23]. We define the aspect ratio of the fitted ellipsoid α, the ratio of the major to the minor axis, as the anisotropy parameter associated with the probability distribution. In the laboratory frame, irrespective of the ϕ and Δt, α remains closer to unity, suggesting the isotropic spread of the particles of the cages around the reference caged-particle [Fig. 2(k)]. However, intriguingly, in the displacement frame, as already visually inferred from the colormaps in Figs. 2(f)–2(i), the shape anisotropy parameter α increases with Δt. The angle-dependent localization of $P(\mathbf{r}_j^{\rm disp}(t_0+\Delta t)|c_j \in C(i,t_0))$ [Fig. 2(j)] and its time-dependent elongation [Fig. 2(k)] thus suggests a strong role of hydrodynamics in governing the evolution of cages, potentially dictating the dynamics of cage breaking (and persistence).

Finally, having established that the shape of the cage is anisotropic in the displacement frame of the reference caged-particle, we now delve into how the particles of the cage rearrange, which either leads to the persistence of the cage or

its breaking and local structural relaxation of the fluid [24,25]. In other words, are there any specific regions in the cage that predominantly help with cage relaxation and persistence? Note, for a reference caged-particle, say i^{th} particle, and its cage particles $C(i, t_0)$, defined at time t_0, a subset of these particles $K(i, t_0, \Delta t)$ will remain part of the cage $C(i, t_0 + \Delta t)$ at later time $t_0 + \Delta t$. This common subset, $K(i, t_0, \Delta t) = C(i, t_0) \cap C(i, t_0 + \Delta t)$, contributes to cage persistence, while particles that were part of $C(i, t_0)$ but are not included in $C(i, t_0 + \Delta t)$, denoted as $\Lambda(i, t_0, \Delta t) = C(i, t_0) \setminus C(i, t_0 + \Delta t)$, contribute to cage breaking [Fig. 3(a)]. Here, "\" denotes the set difference. As expected, the set of particles that remain part of the cage, $k_j \in K(i, t_0, \Delta t)$, exhibit lower mean squared displacements, $\langle \Delta \mathbf{r}^2(\Delta t) \rangle = \langle \frac{1}{N} \sum_j^N (\mathbf{r}_j(t_0 + \Delta t) - \mathbf{r}_j(t_0))^2 \rangle_{t_0}$, than those that leave the cage, $\lambda_j \in \Lambda(i, t_0, \Delta t)$ (Fig. S1 of the SM [22]).

Thus, to investigate if particles in certain spatial regions of the cage are more likely to contribute to cage persistence, we analyze $P(\mathbf{r}_j^{\text{disp}}(t_0) | k_j \in K(i, t_0, \Delta t))$ and $P(\mathbf{r}_j^{\text{disp}}(t_0 + \Delta t) | k_j \in K(i, t_0, \Delta t))$. We find that at t_0, particles that are located in the direction of the displacement of the reference caged-particle have a higher likelihood of remaining part of the cage of the same particle at $t_0 + \Delta t$ [Fig. 3(b) and Video 2 of the SM [22]]. At $t_0 + \Delta t$, however, the common particles of the cage at t_0 and $t_0 + \Delta t$ are more likely to be found in the transverse direction of the reference caged-particle [Fig. 3(c) and Video 2 of the SM [22]].

To further corroborate these arguments, we have only considered a subset of $K(i, t_0, \Delta t)$ such that they lie within an angular region of $\pm 15^\circ$ with respect to the direction of displacement of the reference caged-particle. Figures 3(d) and 3(e) clearly show that common cage particles rearrange in a distinctive "mushroom cloud" pattern, rearranging their positions vertically and moving opposite to the direction of the reference caged-particle's displacement. Conversely, the uncommon particles of the cage, initially distributed opposite to the displacement direction at t_0, become more diffused at $t_0 + \Delta t$ [Figs. 3(f) and 3(g) and Video 2 of the SM [22]]. This indicates that cage breaking and structural relaxation are predominantly facilitated by particles of the cage that are in the regions opposite to the reference caged-particle's motion.

In summary, our experiments represent a first-of-its-kind unraveling of the coarse-grained microscopic dynamics of rigidly confined colloidal fluids, focusing on the dynamic restructuring of particle cages. We demonstrate that, in the laboratory frame of reference, cages evolve isotropically and symmetrically. However, in the displacement frame associated with the motion of the reference caged-particle, the evolution dynamics of the cages are markedly different, becoming anisotropic and asymmetric. Particles that initially form the cage and are positioned ahead of the reference particle reorganize and diffuse transversely to the displacement direction of the caged-particle, while still remaining a part of the cage at a later time, thereby contributing to the persistence of the cage. Conversely, particles behind the reference caged-particle tend to diffuse further away, primarily leading to cage breaking and facilitating the structural relaxation of the fluid.

Intriguingly, our findings show that the cage relaxation timescales, determined solely by the persistence of the

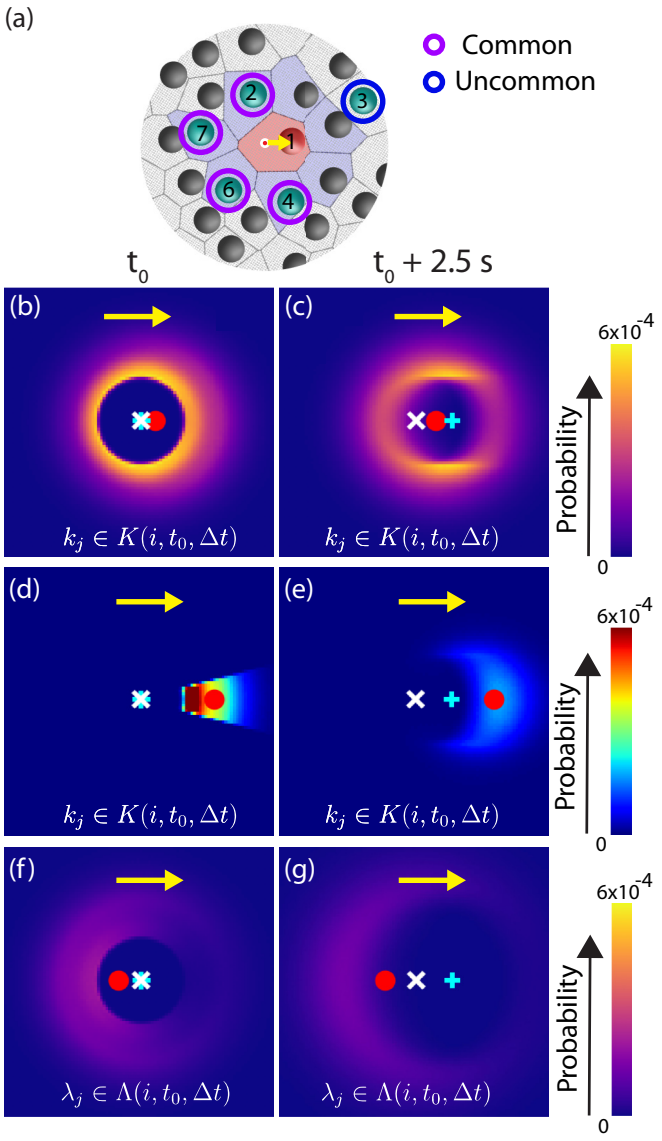

FIG. 3. Distinct anisotropic spatial probability distribution of the cage particles leading to cage persistence and relaxation. (a) Rendering from the experiments of a portion of the field of view, transformed to its respective displacement frame, illustrating the classification of cage particles (cyan spheres) at time t_0 into common $K(i, t_0, \Delta t)$ and uncommon $\Lambda(i, t_0, \Delta t)$ subsets based on their presence or absence in the cage defined for the same reference particle (red sphere) a later time $t_0 + \Delta t$. The common and uncommon cage particles are circled in purple and blue, respectively. Colormap, (b) $P(\mathbf{r}_j^{\text{disp}}(t_0) | k_j \in K(i, t_0, \Delta t))$ and (c) $P(\mathbf{r}_j^{\text{disp}}(t_0 + \Delta t) | k_j \in K(i, t_0, \Delta t))$, at t_0 and $t_0 + \Delta t$, respectively, for $\phi = 0.35$ and $\Delta t = 2.5$ s. (d) and (e) are the same as (b) and (c), respectively, but considering only the subset of particles within an angular region of $\pm 15^\circ$ with respect to the direction of displacement of the reference-caged particle. (f) and (g) depict the same as (b) and (c) but for the uncommon cage particles, $\Lambda(i, t_0, \Delta t)$. Solid red circles in (b)–(g) represent the mean of the probability distributions. White cross and cyan plus symbols in (b)–(g) show the mean position of the particles forming the cage at t_0, and the mean position of the reference caged-particle (either at t_0 or $t_0 + \Delta t$), respectively. Yellow arrows in (b)–(g) depict the displacement direction of the reference caged-particle.

fraction of cage particles over time, remains independent of the packing area fractions examined in this study. However, even a coarse-grained depiction of liquid should exhibit a slowing down of dynamics with increasing ϕ. In fact, for $\phi \geqslant 0.58$, the cage relaxation timescales are observed to be longer than those observed for $\phi \leqslant 0.35$ (Fig. S2 of the SM [22]). In light of this, it would be valuable to investigate whether this indicates a potential dynamic phase transition within the liquid regime. Additionally, considering contrasting strengths, which is $\phi-$dependent, and the phase difference between different hydrodynamic motional modes in q2D [18], this suggests the possibility of different mechanisms of structural relaxation at different ϕ for rigidly confined colloidal fluids. While our study focused on cage dynamics in q2D rigid confinement, it would be worthwhile to explore the coarse-grained dynamics at the lengthscales of cages in suspensions of particles at interfaces [11,26] and those confined on curved surfaces [27,28]. Future studies could also investigate systems with broken ergodicity, such as jammed or glassy states [29–31], as well as active matter, which may exhibit non-trivial cage relaxation dynamics [32]. Moreover, exploring systems with soft and anisotropic particles could provide further insights, as these introduce ruggedness into the energy landscapes, even in two-dimensional contexts [33–35].

We are grateful for the useful discussions with Sivasurender Chandran, B. Prasanna Venkatesh, Adhip Agarwala, and K. Hima Nagamanasa. We gratefully acknowledge financial support from the Department of Science and Technology (Government of India), INSPIRE fellowship IF200274 (N.H.B.), research initiation grant from IIT Gandhinagar through IP/IITGN/PHY/CM/2021/11 (C.K.M.), and the Start-up Research Grant of Science and Engineering Research Board of Government of India through SRG/2021/001077 (C.K.M.).

[1] P. M. Reis, R. A. Ingale, and M. D. Shattuck, Caging dynamics in a granular fluid, Phys. Rev. Lett. **98**, 188301 (2007).

[2] P. Gallo, F. Sciortino, P. Tartaglia, and S.-H. Chen, Slow dynamics of water molecules in supercooled states, Phys. Rev. Lett. **76**, 2730 (1996).

[3] R. Sahu, M. Sharma, P. Schall, S. M. Bhattacharyya, and V. Chikkadi, Structural origin of relaxation in dense colloidal suspensions, arXiv:2403.02517.

[4] B. Li, K. Lou, W. Kob, and S. Granick, Anatomy of cage formation in a two-dimensional glass-forming liquid, Nature (London) **587**, 225 (2020).

[5] E. R. Weeks and D. A. Weitz, Properties of cage rearrangements observed near the colloidal glass transition, Phys. Rev. Lett. **89**, 095704 (2002).

[6] E. Rabani, J. D. Gezelter, and B. J. Berne, Direct observation of stretched-exponential relaxation in low-temperature Lennard-Jones systems using the cage correlation function, Phys. Rev. Lett. **82**, 3649 (1999).

[7] R. A. Quinn and J. Goree, Particle interaction measurements in a Coulomb crystal using caged-particle motion, Phys. Rev. Lett. **88**, 195001 (2002).

[8] C. Mayer, E. Zaccarelli, E. Stiakakis, C. Likos, F. Sciortino, A. Munam, M. Gauthier, N. Hadjichristidis, H. Iatrou, P. Tartaglia *et al.*, Asymmetric caging in soft colloidal mixtures, Nat. Materials **7**, 780 (2008).

[9] V. E. Debets, X. M. De Wit, and L. M. C. Janssen, Cage length controls the nonmonotonic dynamics of active glassy matter, Phys. Rev. Lett. **127**, 278002 (2021).

[10] H. Zhang, Q. Zhang, F. Liu, and Y. Han, Anisotropic-isotropic transition of cages at the glass transition, Phys. Rev. Lett. **132**, 078201 (2024).

[11] B. Illing, S. Fritschi, H. Kaiser, C. L. Klix, G. Maret, and P. Keim, Mermin–wagner fluctuations in 2D amorphous solids, Proc. Natl. Acad. Sci. USA **114**, 1856 (2017).

[12] S. Vivek, C. P. Kelleher, P. M. Chaikin, and E. R. Weeks, Long-wavelength fluctuations and the glass transition in two dimensions and three dimensions, Proc. Natl. Acad. Sci. USA **114**, 1850 (2017).

[13] X. Zheng and J. Earnshaw, On the Lindemann criterion in 2D, Europhys. Lett. **41**, 635 (1998).

[14] H. Shiba, P. Keim, and T. Kawasaki, Isolating long-wavelength fluctuation from structural relaxation in two-dimensional glass: cage-relative displacement, J. Phys.: Condens. Matter **30**, 094004 (2018).

[15] E. Flenner and G. Szamel, Fundamental differences between glassy dynamics in two and three dimensions, Nat. Commun. **6**, 7392 (2015).

[16] Y.-W. Li, C. K. Mishra, Z.-Y. Sun, K. Zhao, T. G. Mason, R. Ganapathy, and M. Pica Ciamarra, Long-wavelength fluctuations and anomalous dynamics in 2-dimensional liquids, Proc. Natl. Acad. Sci. USA **116**, 22977 (2019).

[17] H. Shiba, T. Kawasaki, and K. Kim, Local density fluctuation governs the divergence of viscosity underlying elastic and hydrodynamic anomalies in a 2d glass-forming liquid, Phys. Rev. Lett. **123**, 265501 (2019).

[18] N. H. Barbhuiya, A. Yodh, and C. K. Mishra, Direction-dependent dynamics of colloidal particle pairs and the Stokes-Einstein relation in quasi-two-dimensional fluids, Nat. Commun. **14**, 5109 (2023).

[19] As reported in an earlier work [18], for $\phi > 0.35$, no direction-dependent influence of hydrodynamics was observed on the diffusivity of colloids in a colloid-pair. Therefore, this study focuses on $\phi \leqslant 0.35$.

[20] J. C. Crocker and D. G. Grier, Methods of digital video microscopy for colloidal studies, J. Colloid Interface Sci. **179**, 298 (1996).

[21] P. A. Burrough, R. A. McDonnell, and C. D. Lloyd, *Principles of Geographical Information Systems* (Oxford University Press, USA, 2015).

[22] See Supplemental Material at http://link.aps.org/supplemental/10.1103/PhysRevE.110.L062602 for tabulated values of cage correlation functions, mean squared displacement of common and uncommon cage particles, cage relaxation dynamics, and captions for supplementary videos.

[23] Method for determining the inner contour of the probability distribution's maxima through ray tracing: Rays are emanated

in all directions and traced from the probability distribution's center (mean) to identify points where the probability is maximum along the ray directions. These points define the contour on which an ellipse is fitted.

[24] Y. Chen, Z. Ye, K. Wang, J. Huang, H. Tong, Y. Jin, K. Chen, H. Tanaka, and P. Tan, Visualizing slow internal relaxations in a two-dimensional glassy system, Nat. Phys. **19**, 969 (2023).

[25] X. Cao, H. Zhang, and Y. Han, Release of free-volume bubbles by cooperative-rearrangement regions during the deposition growth of a colloidal glass, Nat. Communications **8**, 362 (2017).

[26] C. van Baalen, J. Vialetto, and L. Isa, Tuning electrostatic interactions of colloidal particles at oil-water interfaces with organic salts, Phys. Rev. Lett. **131**, 128202 (2023).

[27] A. Bausch, M. J. Bowick, A. Cacciuto, A. Dinsmore, M. Hsu, D. Nelson, M. Nikolaides, A. Travesset, and D. Weitz, Grain boundary scars and spherical crystallography, Science **299**, 1716 (2003).

[28] N. Singh, A. Sood, and R. Ganapathy, Observation of two-step melting on a sphere, Proc. Natl. Acad. Sci. USA **119**, e2206470119 (2022).

[29] P. Charbonneau, A. Ikeda, G. Parisi, and F. Zamponi, Dimensional study of the caging order parameter at the glass transition, Proc. Natl. Acad. Sci. USA **109**, 13939 (2012).

[30] P. Charbonneau, Y. Jin, G. Parisi, and F. Zamponi, Hopping and the Stokes-Einstein relation breakdown in simple glass formers, Proc. Natl. Acad. Sci. USA **111**, 15025 (2014).

[31] P. K. Morse and E. I. Corwin, Geometric signatures of jamming in the mechanical vacuum, Phys. Rev. Lett. **112**, 115701 (2014).

[32] R. Ni, M. A. C. Stuart, and M. Dijkstra, Pushing the glass transition towards random close packing using self-propelled hard spheres, Nat. Commun. **4**, 2704 (2013).

[33] X. Yang, R. Liu, M. Yang, W.-H. Wang, and K. Chen, Structures of local rearrangements in soft colloidal glasses, Phys. Rev. Lett. **116**, 238003 (2016).

[34] Z. Zheng, F. Wang, and Y. Han, Glass transitions in quasi-two-dimensional suspensions of colloidal ellipsoids, Phys. Rev. Lett. **107**, 065702 (2011).

[35] C. K. Mishra and R. Ganapathy, Shape of dynamical heterogeneities and fractional Stokes-Einstein and Stokes-Einstein-Debye relations in quasi-two-dimensional suspensions of colloidal ellipsoids, Phys. Rev. Lett. **114**, 198302 (2015).